

Investigation of multispectral imaging algorithm for temperature determination on a numerical experiment platform in Laser-based Powder Bed fusion of Metals

Untersuchung des multispektralen Bildgebungsverfahrens zur Temperaturbestimmung auf einer numerischen Experimentierplattform beim Laserbasierten Pulverbett-Schmelzverfahren von Metallen.

Semester Thesis

at the Department of Mechanical Engineering of the Technical University of Munich

Supervised by	Prof. Dr.-Ing. Katrin Wudy M.Sc. Ruihang Dai Laser-based Additive Manufacturing
Submitted by	Zhaoyong Wang Connollystr.3 80809 München
Submitted on	July 31, 2023 in Garching

Scope of Work

Title of the Semester Thesis:

Investigation of multispectral imaging algorithm for temperature determination on a numerical experiment platform in Laser-based Powder Bed fusion of Metals

Author: B.Sc. Zhaoyong Wang

Issuance: 15.03.2023

Supervisor: M.Sc. Ruihang Dai

Submission: 31.12.2021

Setting:

Laser-based Powder Bed Fusion of Metals (PBF-LB/M) is an additive manufacturing process which produces components with a laser by successively melting metal powders applied in layers. This additive manufacturing process offers the advantage of a complex lightweight design. However, complicated thermal histories during laser-metal interaction can lead to process defects such as keyholing. Since the process is thermally driven, acquiring the absolute temperature distribution in the laser-material interaction zone is vital to gain a deeper understanding of the process. However, no measurement system in PBF-LB/M is currently available to determine the absolute temperature due to unknown emissivity. Multispectral Imaging (MSI) has the potential to determine the absolute temperature and emissivity simultaneously by capturing multiple wavelengths of radiance from the melt pool.

Objective:

This work aims to optimize the MSI algorithm to determine the absolute temperature accurately. Since the mapping between the digital value and radiance still needs to be investigated, direct optimization of the MSI algorithm based on the experimental data is challenging. Therefore, the first step is to develop a virtual experiment to obtain "ideal" radiance determined by the given temperature distribution and emissivity. This way, the MSI algorithm can be optimized based on the input and calculated temperature and emissivity. The virtual experiment platform will also allow for the investigation of various temperature distributions and emissivity models in a time- and cost-efficient manner.

Methodology:

The content of the present thesis can be subdivided into the following tasks

- Literature review regarding MSI, material emissivity model and curve fitting algorithms
- Development of a virtual experiment platform
- Generate virtual experiments with various emissivity models and temperature fields
- Optimization of the MSI algorithm based on virtual experiments
- Scientific documentation of the results

Declaration

I hereby confirm that this semester thesis was written independently by myself without the use of any sources beyond those cited, and all passages and ideas taken from other sources are cited accordingly.

.....
Location, Date

.....
Signature

With the supervision of Mr. Zhaoyong Wang by Mr. Ruihang Dai intellectual property of the Professorship Laser-based Additive Manufacturing (LBAM) flows into this work. A publication of the work or a passing on to third parties requires the permission of the head of the professorship. I agree to the archiving of the printed thesis in the LBAM library (which is only accessible to LBAM staff) and in LBAM's digital thesis database as a PDF document.

.....
Location, Date

.....
Signature

Abstract

temperature is one of the most important parameters in PBF-LB/M. so, monitoring the temperature at melt pool necessary. in oder to archieve this, a numerical experiment platform is formed. then parameter is calculated

Zusammenfassung

Hier könnte Ihre Kurzzusammenfassung stehen.

Contents

1	Introduction	1
2	State of the art	3
2.1	Process monitoring	3
2.2	Multispectral imaging	3
2.3	Emissivity model	3
2.4	Temperature field in Laser-based Powder Bed Fusion	3
2.5	Motivation of this thesis	3
3	Theory and methodology	5
3.1	Physical value of radiation	5
3.2	Virtual experiment platform	7
3.3	Camera model	7
3.3.1	Frequency response	7
3.3.2	Integration method	9
3.3.3	Implementation	10
3.4	Temperature estimation algorithm	11
3.5	Emissivity model in temperature estimation algorithm	12
4	Application	13
4.1	Experiment data generation	13
4.1.1	Temperature field	14
4.1.2	Emissivity model	15
4.1.3	Camera model	19
4.2	Temperature estimation algorithm	19
4.2.1	Rebuild physical value of spectral radiation intensity	20
4.2.2	Emissivity model used for calculation	20
4.2.3	Curve fit algorithm	22
4.2.4	Parameters in temperature estimation algorithm	23
5	Calcualtion results and analysis	25
5.1	Calculation results	25
5.1.1	Raw experiment data from virtual experiment platform	25
5.1.2	Estimated temperature field and emissivity field	28
5.1.3	Statistical results	30
5.2	Data analysis	35
5.2.1	Sensitivity analysis of emissivity models	35
5.2.2	Performance between different materials	35
6	Conclusion and prospects	37
A	Appendices	39
	Bibliography	41
	List of Abbreviations	43

1 Introduction

Additive Manufacturing (AM) is a different type of processing technology to conventional manufacturing methods. Instead of removing material from the raw part, additive manufacturing is usually described as "a process of joining materials to make objects layer by layer or element by element"[1]. It is a useful method for reducing the the duration from product design to product manufacturing and imporving the material utilization[2].

There are several AM technologies that can be sorted into different categories. Laser-based Powder Bed Fusion of Metals (PBF-LB/M), which also called Selective Laser Sintering (SLS), is one of the powder based AM processes[3]. In this process, a laser beam with high energy density is focused onto the surface of a metal powder bed, which was heated up to a temperature near the melt temperature. Then, the metal powder is melted and form the upper surface of the object. Last, the building platform will go downwards to build next layer. This process will be repeated until the desired object is built[4].

Since the process is based on the phase change of materials, processing parameters such as laser power, layer thickness, hatch distance and scanning strategies are critical for producing dense materials, minimize defects, improve surface quality and build rate[5]. The common denominator between them is that the parameters of the process are varied by controlling the temperature profile of the metal powder[2]. Thus, the importance of obtaining the temperature information on the surface layer is high.

The solidification front of metal powders moves with a high velocity (generally $0.01 \sim 10 \text{ m/s}$)[6], the cooling rate of material is normally at range of $10^5 \sim 10^6 \text{ K/m}$ [5]. Thus, a contactless temperature measurement is required to obtain the temperature of the surface area.

Two different methods is used for monitoring the surface temperature in recent studies, namely conventional infrared irradiation temperature measurement methods and multi-wavelength techniques[7]. Infrared irradiation technique is cost-effective, but it requires information about the emissivity of the material[8]. On the contrary, a multi-color pyrometer with a specific wavelength range could be used in the case of changing emissivity[9]. In this thesis, a virtual experiment platform using a multispectral imaging algorithm is developed to simulate the output behavior of a spectral pyrometer.

After obtaining the radiation image, a curve fit algorithm is applied to estimate the temperature field of the image and emissivity field simultaneously. This semester thesis aims to develop a stable temperature estimation program based on curve-fit algorithm. With the results obtained from the virtual experiment platform, the performance of the temperature estimation algorithm is verified.

2 State of the art

haha[10]

2.1 Process monitoring

2.2 Multispectral imaging

2.3 Emissivity model

2.4 Temperature field in Laser-based Powder Bed Fusion

2.5 Motivation of this thesis

3 Theory and methodology

As mentioned in previous sections, forming a virtual experiment platform is necessary for investigating the temperature estimation algorithm. So, a virtual experiment platform is developed based on Planks'law, then, a virtual multi-spectral pyrometer is applied to obtain the digital value (also called image).

3.1 Physical value of radiation

Radiation is emitted from any object with a temperature above 0 K. In equation 3.1 can be found, that the radiation depends on the black body radiation $B(\lambda, T)$ and emissivity $\varepsilon(\lambda, T)$. Both value are temperature T and wavelength λ dependent.

$$L(\lambda, T) = B(\lambda, T) \cdot \varepsilon(\lambda, T) \quad (3.1)$$

By Plank's Law, black body radiation can be described in Eq.3.2,

$$B(\lambda, T) = \frac{2hc^2}{\lambda^5} \cdot \left[\exp\left(\frac{hc}{\lambda k_B T}\right) - 1 \right]^{-1} \quad (3.2)$$

With absolute temperature T , wavelength λ , speed of light c , Plank constant h and Boltzmann constant k_B . Black body radiation is irrelevant to the material itself, all materials at the same temperature have the same spectral black body radiation.

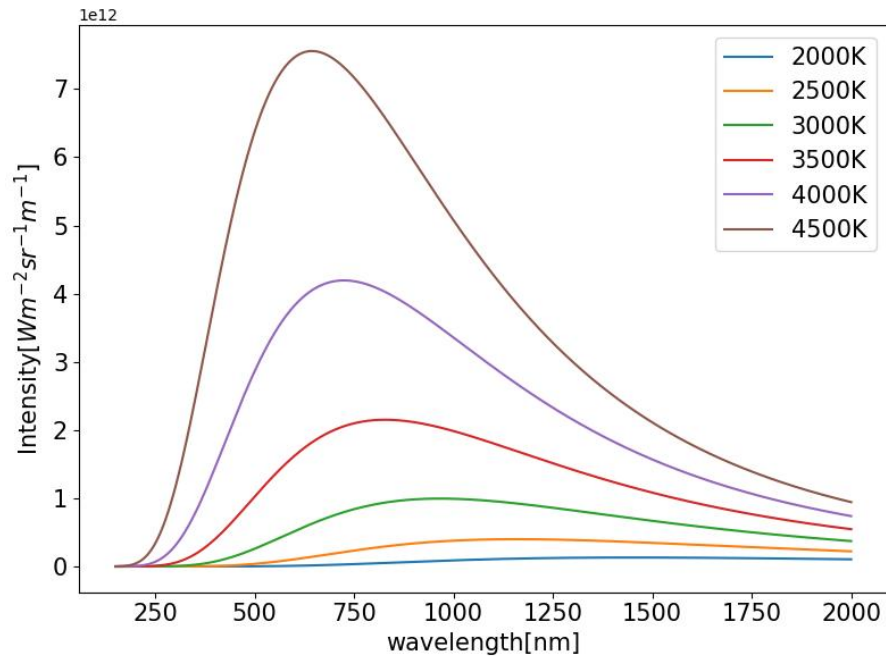


Figure 1: Black body radiation of materials with different temperature

Fig.1 illustrates the spectral radiation intensity of a blackbody at different temperatures. It can be observed that the spectral radiation intensity exhibits a peak at a specific wavelength.

According to Wien's displacement law, the relationship between the wavelength of the peak λ_{peak} and temperature T can be described in Eq.3.3:

$$\lambda_{peak} = \frac{b}{T} \quad (3.3)$$

With Wien's displacement constant $b = 2898 \mu m \cdot K$, it can be found that the wavelength of this peak decreases as the temperature rises.

From this, it can be concluded that the shape of the blackbody's spectral radiation intensity varies with temperature. This is evident in two aspects: firstly, the position at which the peak appears, and secondly, the distribution of spectral radiation intensity along the wavelength. Indeed, this characteristic provides the possibility to determine the temperature of a blackbody material in reverse, i.e., by calculating the temperature based on the known spectral radiation intensity.

On the contrary, emissivity varies from material to material. It is the ratio of the actual spectral intensity emitted by the object to the spectral intensity of the black body radiation. In the study of radiation, two idealized material models are generally used to describe the idealized properties of radiation, namely black body and grey body.

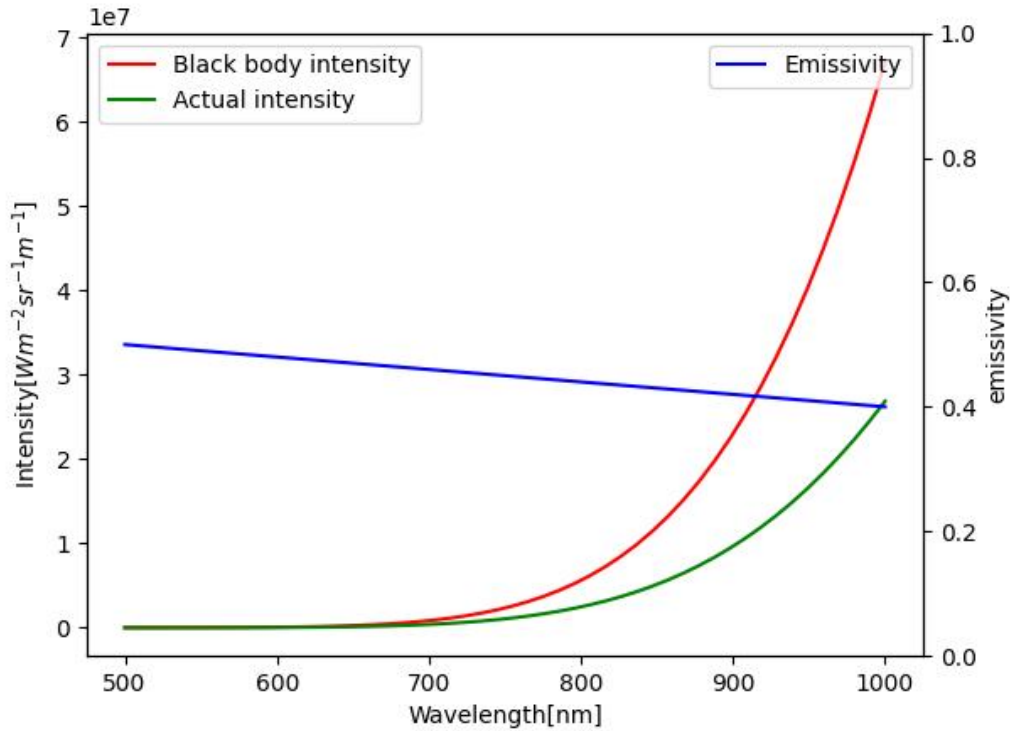


Figure 2: Black body radiation, emissivity and real radiation of an example normal material at 1000K

Black-body material emits electromagnetic black body radiation, which is irrelevant to the wavelength of the radiation and the shape of the material[11]. Which also means the emissivity of a black body is constantly 1. It could be used to validate the temperature estimation algorithm in following sections.

Unlike black-body materials, grey-body materials have an emissivity between 0 and 1. Not all of the thermal radiation could be emitted to the outside of the material. Different from

normal materials, the emissivity of a grey-body material is irrelevant to the wavelength of radiation.

In Fig.2 can be found, that the real spectral intensity of a normal material is lower than the black body spectral intensity. And the emissivity of the material varies with the increase of the radiation wavelength.

It can be seen that the construction of a reliable emissivity model is crucial to the accuracy of the virtual experimental platform. It is the key component used to generate the experimental data.

3.2 Virtual experiment platform

After obtaining the physical spectral intensity of the material, a virtual experiment platform is used to transform the physical value into digital value, which simulate the behavior of a real spectral pyrometer. As described in Fig.3a, a camera with a lens system focused on the surface of the powder bed is responsible for obtaining spectral radiation of the heated metal powder. It can be seen from Fig.3b, each pixel of the sensor contains 8 filters and thus be able to obtain 8 intensity digital values in different channels. Thus, a virtual experiment platform with the same structure as the real experiment platform is built.

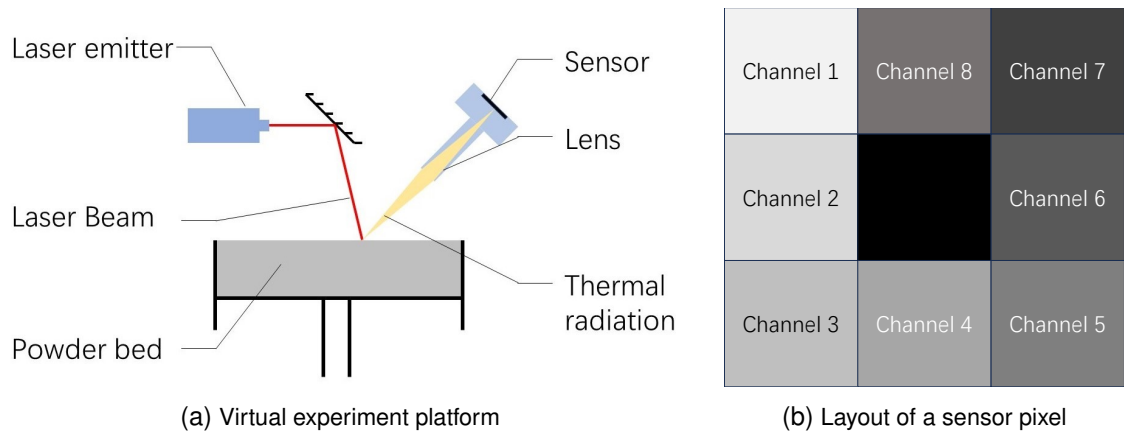


Figure 3: Structure of the virtual experiment platform and Layout of a sensor pixel

3.3 Camera model

It can be found in Fig.3, The thermal radiation is emitted from the surface of powder bed, and passes through the lens system of the camera, finally, it reaches the sensor and be converted into digital values. The simplified process can be seen in Fig.4. As dA_m is the area of the focused surface and dA_{pixel} the area of the pixel in camera system, n_m is the normal vector of the surface.

3.3.1 Frequency response

After obtaining the virtual experiment platform and knowing the external setup of the sensor, the internal effects of the camera system should also be taken into account in the complete virtual experiment platform.

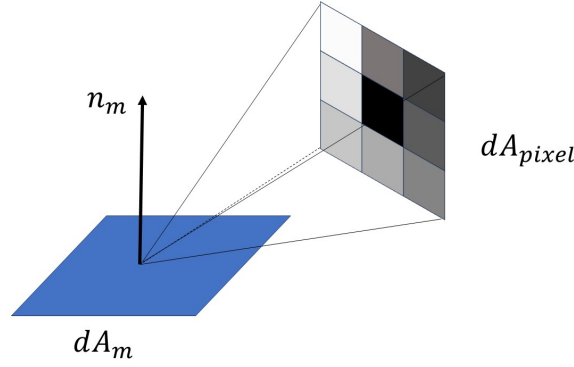


Figure 4: Radiative exchange between camera system and powder bed

In order to simulate real camera system, the frequency response of sensor and lens should be considered. In real camera systems, all spectral radiation will pass through the lens system of camera. Since the lens system is not an idealized system, the effect of the lens system is not negligible.

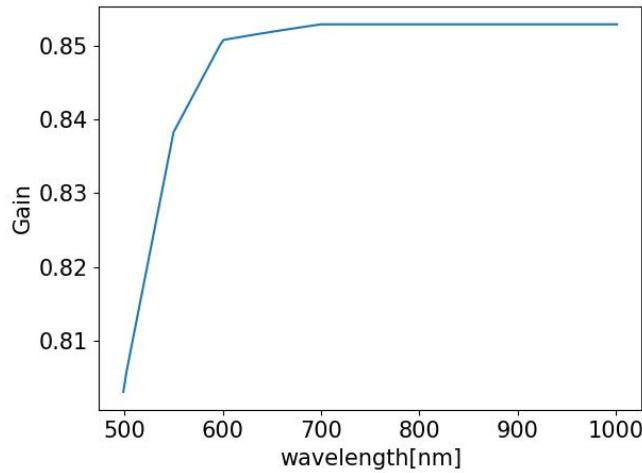


Figure 5: Frequency response of the lens system

It can be found in Fig.5 that system gain of lens system is not constant. In the wavelength range of 500 to 700 nanometers, the lens is more sensitive to the radiation with long wavelength. With the increasing wavelength, the system gain of the lens system keep constant at 0.853.

In addition to the fact that the lens system respond differently to radiation with different wavelengths, the sensor of the camera also have wavelength-dependent quantum efficiency. As mentioned in previous section, the acquisition of the spectral intensity by the sensor for different channels is based on the filter before the pixels.

Fig.6 shows the quantum efficiency of the camera sensor in different channels. Unlike an ideal sensor that receives only single wavelength radiation, the intensity information received by a real sensor is a combination of a spectral radiation and 8 filters with different frequency responses. Thus, the camera system is able to obtain the spectral radiation intensity in 8 channels simultaneously.

To make the virtual experiment platform more comparable to real experiments, it can be

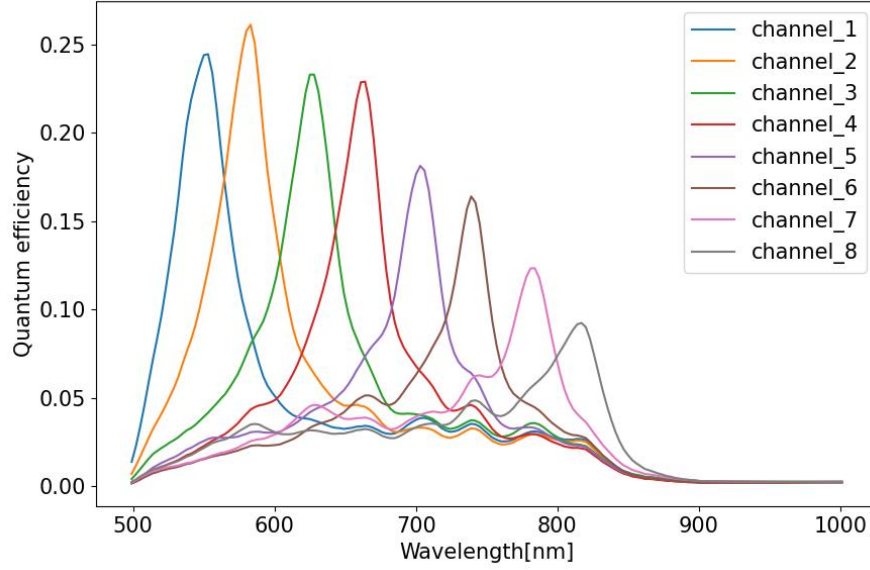


Figure 6: Quantum efficiency of camera system in each channel

concluded that it is necessary to build a camera model that incorporates the effects of sensor quantum efficiency and lens transparency. Then, the physical value of the spectral radiation intensity could be calculated accurately by the digital value of spectral radiation intensity obtained from the virtual experiment platform.

3.3.2 Integration method

As a result, the process of converting the physical values of radiation intensity into digital values needs to be accurately reproduced. Since the total efficiency of the camera (η_{camera}) was delivered by quantum efficiency ($\eta_{quantum}$) of the sensor and transparency of the lens system (τ_{lens}), the mathematical relationship could be described in Eq.3.4.

$$\eta_{camera} = \eta_{quantum} \cdot \tau_{lens} \quad (3.4)$$

Fig.7 shows the relationship between the incoming spectral radiation intensity and actual captured spectral radiation intensity by the camera system. It can be found that the wavelength of the spectral radiation intensity actually received by the sensor deviates from the wavelength of the spectral radiation intensity it supposed to receive.

Obtaining the physical value of spectral radiation intensity, the sensor is responsible for transforming the physical value into digital value for upcoming proceedings. The camera system used in real experiment platform uses Charge-coupled device (CCD) or Complementary Metal-oxide Semiconductor (CMOS) as their sensors. Both sensors transform the photon flux $\phi(\lambda)$ incident on the semiconductor into photocurrent I_{ph} [12].

$$I_{ph} = q \int_{\lambda} \phi(\lambda) \cdot \eta_{camera}(\lambda) d\lambda \quad (3.5)$$

With a certain temperature T :

$$\phi(\lambda) = L(\lambda, T) \quad (3.6)$$

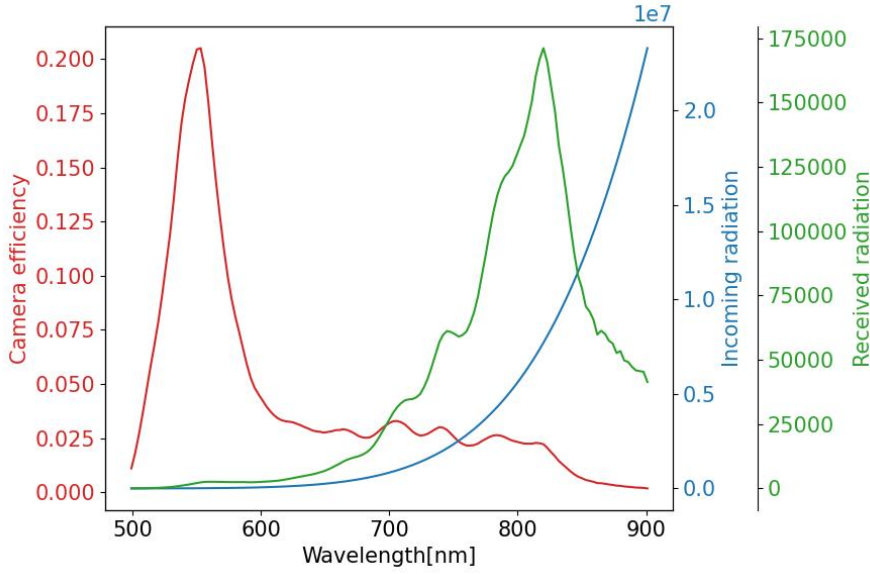


Figure 7: Actual received spectral radiation intensity by channel 1 at 1000K

Eq.3.5 is the mathematical description of the transformation. Where $\phi(\lambda)$ denotes photon flux on the sensor, which is equal to the spectral radiation intensity on the sensor $L(\lambda, T)$ as described in Eq.3.6, and $\eta_{camera}(\lambda)$ denotes the total efficiency of the camera in Eq.3.4. q is the sensitivity parameter of the sensor.

3.3.3 Implementation

Similar to the method used to obtain the digital value of spectral radiation intensity in the real experiment, the virtual experiment platform calculates the intensity digital value in 8 channels using the virtual camera by entering the material properties of the point being measured.



Figure 8: Procedure of using virtual experiment platform to generate digital values

Fig.8 shows the working procedure of the virtual experiment platform. To enable the virtual experimental platform to run on various devices, the entire platform has been implemented using Python as the programming language and packaged into a .py file. Furthermore, all functions have been vectorized to facilitate the generation of image outputs resembling those captured by a physical camera. Additionally, the parallel computing package in Python has been utilized to minimize computation time.

3.4 Temperature estimation algorithm

After obtaining the experimental data calculated by the virtual experiment platform, a temperature estimation algorithm should be developed to calculate the temperature of the measured point based on the experimental data.

Similar to the set up in real experiments, the parameters of the camera model can be considered as known in the virtual experimental platform mentioned in this article. This will on the one hand improve the accuracy of the temperature estimation algorithm and on the other hand avoid some unnecessary complexity.

Thus, in this temperature estimation algorithm, the known variable is the digital value of spectral intensity captured by camera model in virtual experiment platform, the characteristic of the camera system. The variables to be estimated are the temperature of the measured point and its emissivity.

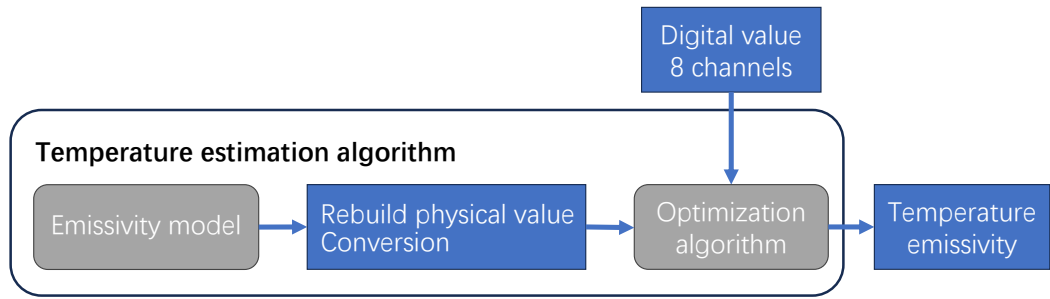


Figure 9: Procedure of temperature estimation algorithm

Fig.9 shows the proceeding procedure of the temperature estimation algorithm. The physical value of the spectral radiation intensity ($I_{rec}(i)$) in the i_{th} channel should be reconstructed in Eq.3.7:

$$I_{rec}(i) = q \int B(\lambda, T) \cdot \varepsilon(\lambda, k, T) \cdot \eta_{camera}(i) d\lambda \quad (3.7)$$

With $I_{rec}(i)$ the reconstructed physical value in i_{th} channel, $B(\lambda, T)$ the black body radiation, $\varepsilon(\lambda, k, T)$ the emissivity model in temperature estimation algorithm, $\eta_{camera}(i)$ the total camera efficiency of i_{th} channel. It can be found that the emissivity model have an additional parameter k , this parameter is used for fitting the emissivity behavior of the measured material. More details can be found in the following section.

Once the reconstruction of the physical value is completed, it is necessary to convert this physical value into a digital value. This conversion process is dependent on the parameter settings of the sensor system, such as exposure time, aperture size of the lens, etc. For the purposes of this paper, it is assumed that the conversion relationship is linear.

Given an initial guess of the status parameters, namely temperature(T_0) and parameters in emissivity model(k_0). Then, an curve fit algorithm is applied to minimize the difference between the reconstructed digital value (I_{rec}) and the actual digital value (I_{act}) in Eq.3.8.

$$\min_{k, T} \sum_{i=1}^8 F(I_{rec}(i), I_{act}(i)) \quad (3.8)$$

$F(I_{rec}(i), I_{act}(i))$ is the cost function of the curve fit algorithm. In this application, Non-linear least squares method is used to obtain the optimum parameters as Eq.3.9.

$$F(I_{rec}(i), I_{act}(i)) = (I_{rec}(i) - I_{act}(i))^2 \quad (3.9)$$

After obtaining the estimated temperature ($T_{estimate}$) and the parameter (k) in the emissivity model, the data will be saved in a .xlsx file for potential operations.

3.5 Emissivity model in temperature estimation algorithm

As an unknown quantity in the temperature estimation algorithm, the nature of emissivity as a function of wavelength also introduces an additional degree of freedom into the overall calculation process. In order to provide a more general description of the trend of emissivity with wavelength, an additional parameter (k) in the emissivity model used for temperature estimation has been introduced.

Due to the inherent complexity of this trend, it is often impossible to describe the emissivity using a single parameter. Therefore, the parameter (k) is normally represented as a vector composed of multiple variables. This approach allows for both a concise mathematical representation and the incorporation of more intricate emissivity models into the temperature estimation algorithm.

4 Application

After the theoretical basis of the virtual experiment platform is known and the program of the virtual experiment platform is built, the application should be verified with experiment data generated based on the real experiment.

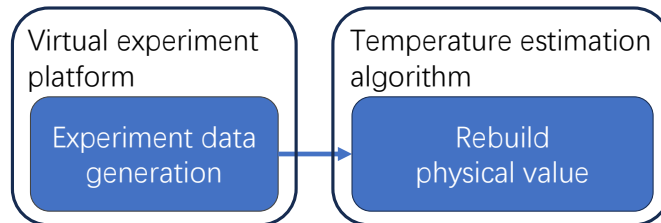


Figure 10: Complete procedure from data generation to model validation

Fig.10 shows the procedure of the application. Firstly, an experiment data set should be generated according to the parameters of the hypothetical material. Then, a temperature estimation algorithm is applied to estimate the temperature of the hypothetical material. Last, a validation procedure is used to check the accuracy and stability of the results of temperature estimation algorithm.

As mentioned in previous sections, these functions is implemented in three programmes. Namely virtual experiment platform, temperature estimation algorithm and validation procedure. Similar to conventional experiment methods, these steps are independent procedures, which means they do not interact with each other.

Accordingly, this chapter will be divided into three sections, which describe the implementation and the parameter settings of the virtual experiment platform, temperature estimation algorithm and validation procedure.

4.1 Experiment data generation

As the first of the three steps mentioned above, it is crucial to generate accurate experimental data correctly. It affects the comparability of the virtual experimental platform with real experiments on the one hand, and the accuracy of the temperature estimation algorithm on the other. As a result, the virtual experimental platform should be able to perform calculations for as many hypothetical materials with different properties as possible.

In order to be able to obtain image similar to image from real camera, the area that the virtual camera is able to capture is set to a 50*50 pixel picture. Fig.11 shows the image obtained from real experiment and virtual experiment platform. The major difference between these two images is the coloring. In real experiment, the raw image was saved as a .tiff file, which obtain the spectral intensity received by the specific channel. Then, the intensity is expressed as brightness of the pixel in the display of the image. This results in the experiment data that is not intuitive and requires specialised software to open these data.

As a result, there are a number of optimisations that have been applied in this virtual

experiment platform. Firstly, the raw digital value of the received spectral intensity was saved in an .xlsx file, which simplifies the reading of the data as well as the conversion. In addition, a .jpg image of each channel similar to the real experiment data is also saved. Different from the real experiment data, colours are used here to indicate the value of the spectral intensity. This improves the readability of the experiment data.

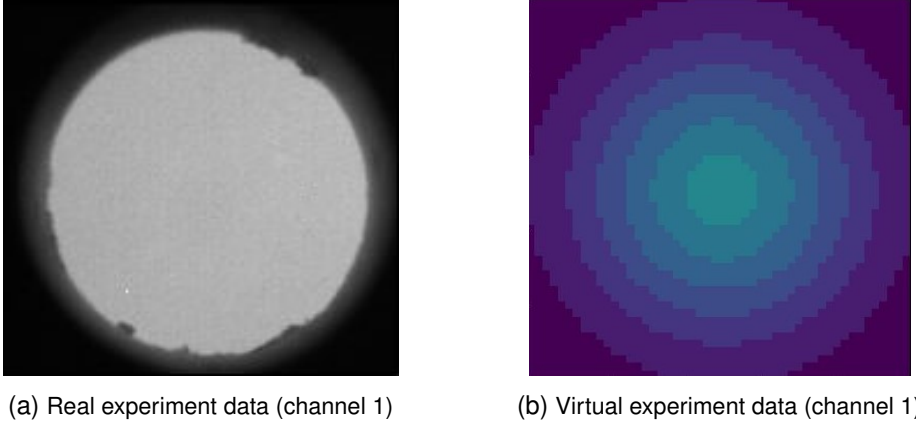


Figure 11: Comparison between real experiment data at 1300K (a) and virtual experiment data at 1098K (b)

Thus, the observation area is obtained by initialization of the the virtual experiment platform. Temperature field, emissivity model of the hypothetical material and the integration method are the parameters to be defined as the next step.

4.1.1 Temperature field

As mentioned in previous sections, temperature is one of the most important parameters in the virtual experiment platform. In order to obtain results similar to real experiments, a temperature field exists in the observation area. For the purpose of simplifying the calculation process, this temperature field consists of two main regions, a background region at the edge of the observation area, where the temperature is uniformly set to 1000K, and an internal high temperature region, where the temperature follows a predefined distribution.

Fig.12 shows three different temperature distribution which are able to be generated by the virtual experiment platform. Namely linear distribution, gaussian distribution and sigmoid distribution. In order to simplify the visualization process, all temperature fields are generated based on the center point of the observation area. As the temperature of each point is calculated based on the normalized distance d_{rel} or absolute distance d_{abs} to the center point of the observation area.

Linear distribution means that the temperature increases linearly from the back ground area to the center point of the observation area. The details can be found in Eq.4.1. This distribution has the potential to demonstrate the spectral radiation behavior of the hypothetical material in different temperature.

$$t = t_{center} + (t_{background} - t_{center}) \cdot d_{rel} \quad (4.1)$$

Gaussian distribution is also called normal distribution. In this distribution type, the temperature field in observation area obeys gaussian distribution described in Eq.4.2. With the temperature of the center point in observation area equals the defined center

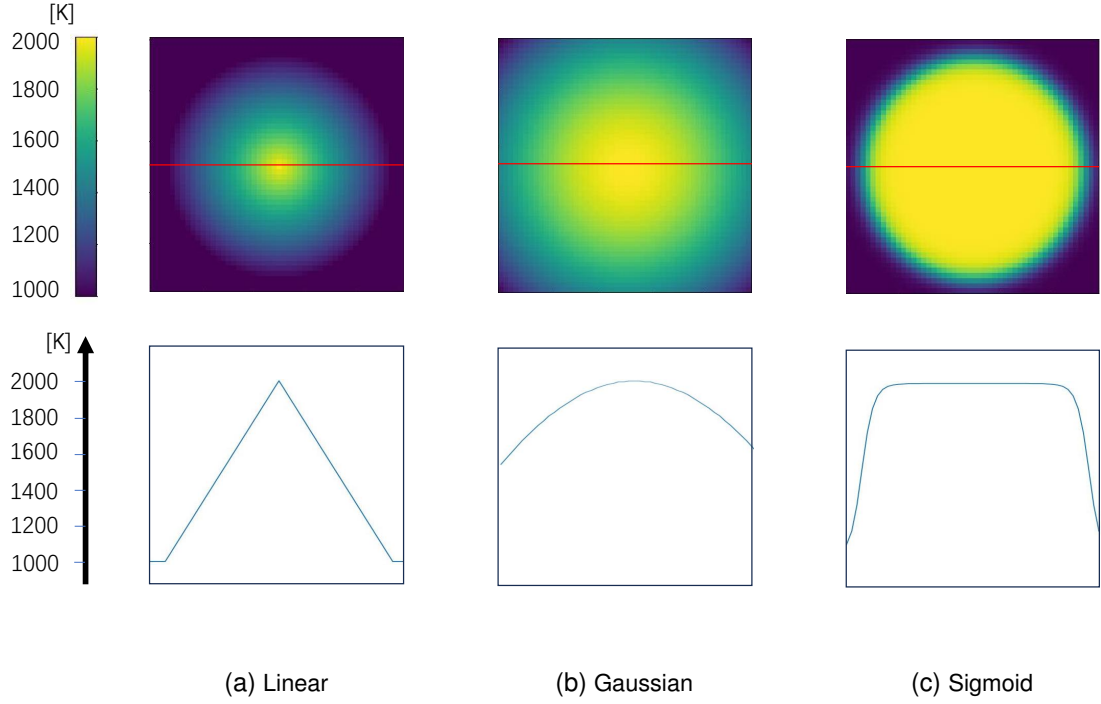


Figure 12: Temperature field of 3 different temperature distribution and the temperature profile in the middle line of the observation area. (a): Linear distribution. (b): Gaussian distribution. (c): sigmoid distribution

temperature. Due to energy input of the system and heat transfer in metal powder, this temperature distribution is more likely to simulate the real situation in experiment.

$$t = t_{center} + (t_{background} - t_{center}) \cdot \exp\left(-\frac{d_{abs}^2}{2 \cdot \sigma^2}\right) \quad (4.2)$$

Different to the temperature field mentioned before, the temperature in the center region of observation area remains constant. The mathematical expression can be found in Eq.4.3:

$$t = t_{center} + (t_{background} - t_{center}) \cdot \text{sigmoid}\left(\left(\frac{d_{abs}^2}{r_{set}^2} + 1\right) \cdot 1000\right) \quad (4.3)$$

With sigmoid function can be found in Eq.4.4:

$$\text{sigmoid}(x) = \left(1 + \exp\left(-\frac{x}{100}\right)\right) \quad (4.4)$$

Sigmoid function gives the opportunity to perform the temperature estimation algorithm in a stable temperature. Thus, the potential to investigate the consistency of the temperature estimation algorithm and performance of the noise cancellation program is given.

4.1.2 Emissivity model

Obtaining temperature field of the hypothetical material, an emissivity model is required to calculate the physical value of spectral radiation intensity emitted from the hypothetical material.

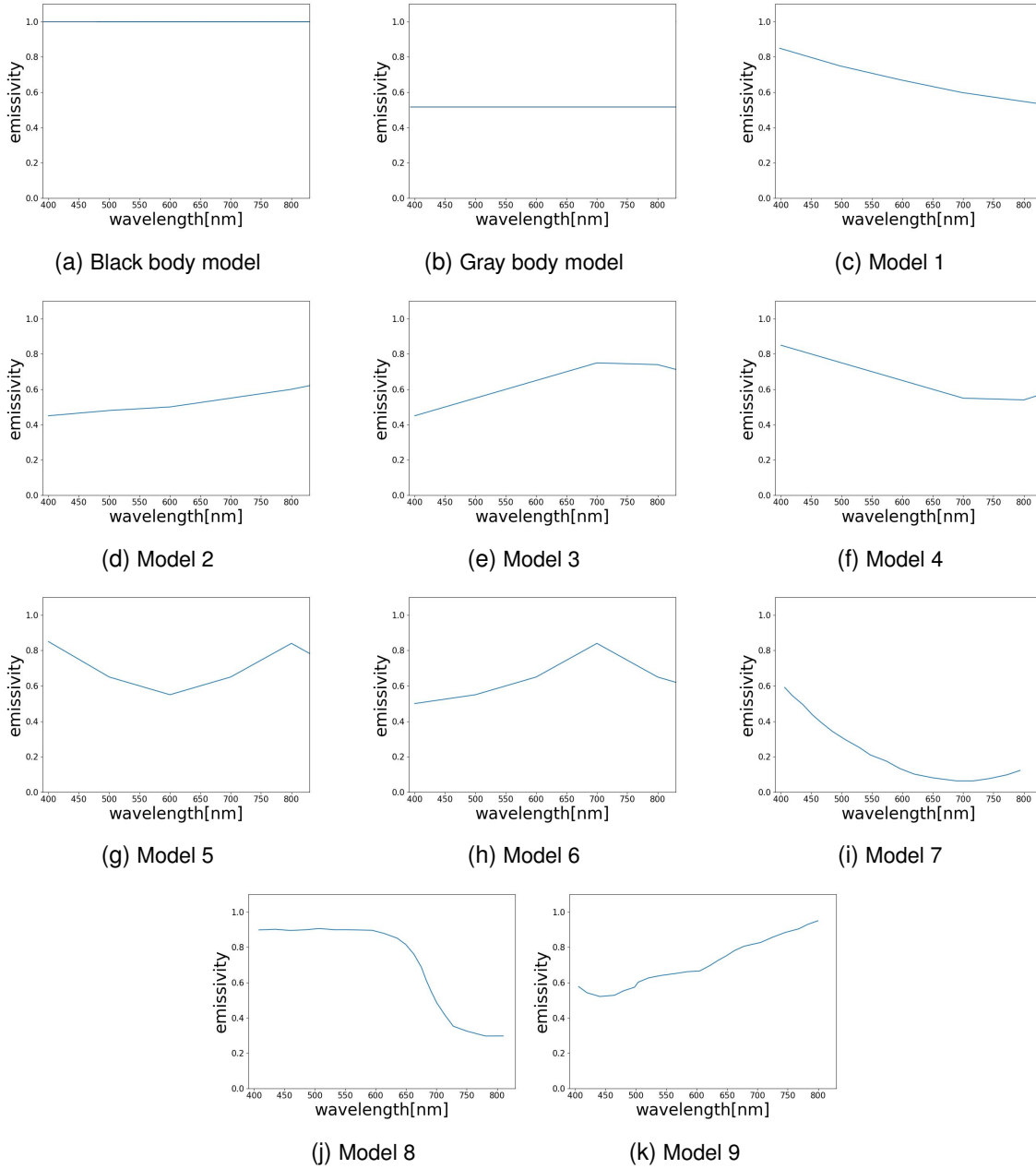


Figure 13: Raw emissivity data used in virtual experiment platform. (a), (b) are black body and gray body; (c) - (h) are hypothetical materials[13]; (i) - (k) are real materials[14].

Since the emissivity of metal powder is wavelength (λ) and temperature (T) relevant, the emissivity model in this virtual experiment platform is formed based on the Eq.4.5.

$$\varepsilon(\lambda, T) = \varepsilon_{raw}(\lambda) \cdot K_T(T) \quad (4.5)$$

The raw emissivity data $\varepsilon_{raw}(\lambda)$ in Fig.13 are obtained by Wang et al.[13] and Taunay et al.[14]. These data sets could be used to simulate the radiation behavior of various hypothetical materials.

Fig.13a and Fig.13b represent blackbody radiation and graybody radiation, respectively. In these two models, emissivity remains constant with respect to temperature and wavelength variations. Consequently, this represents the simplest emissivity model.

Models 1 to 6 describe the emissivity of different hypothetical materials. Model 1 represents the case of monotonically decreasing emissivity, which is also consistent with the emissivity model of iron. Model 2 describes a scenario where emissivity increases with wavelength. Models 3 and 4 represent emissivity as a convex and concave curve. Model 5 depicts a situation where emissivity exhibits two inflection points as wavelength increases. Lastly, Model 6 illustrates a scenario where emissivity shows a single inflection point as wavelength increases. One of the advantages of using a virtual experiment platform is the ability to test a greater diversity of hypothetical materials than what may be feasible in real experiments.

After obtaining the raw data on the relationship between emissivity and wavelength, the dependence of emissivity on temperature is characterised as a temperature factor $K_T(T)$ in Eq.4.6.

$$K_T(T) = \begin{cases} 1 - T_{ref} \cdot 0.2 & T < T_{melt} \\ (1 - T_{ref} \cdot 0.2) \cdot 0.1 & T \geq T_{melt} \end{cases} \quad (4.6)$$

With

$$T_{ref} = \frac{T - T_{lb}}{T_{ub} - T_{lb}} \quad (4.7)$$

This temperature factor describes the tendency of emissivity to decrease with increasing temperature between T_{lb} and T_{ub} , on the other hand, it also describes the change of emissivity due to the phase change of the hypothetical material that occurs at melting temperature T_{melt} .

Fig.14 shows the emissivity model based on model 9 in different temperature and wavelength. It can be found that the emissivity at a temperature below melting temperature (1700K) varies significantly with wavelength. This is caused due to the raw emissivity data. Then, at liquid phase of the hypothetical material, emissivity decreases to a value lower than 0.1.

Thus, the phase change phenomenon of hypothetical material is also characterized, which gives the virtual experiment platform more potential to simulate real experiments.

In contrast to hypothetical materials, the emissivity of real iron is influenced by various factors, such as impurity content, surface roughness, and the content of iron oxide. However, these factors are not within the scope of discussion in this work. Therefore, for the verification part, data from literature sources on pure iron were chosen [15], [16]. Fig.15 illustrates the variation of emissivity for pure iron with respect to wavelength and temperature. It can be observed that the emissivity of real materials shows a relatively

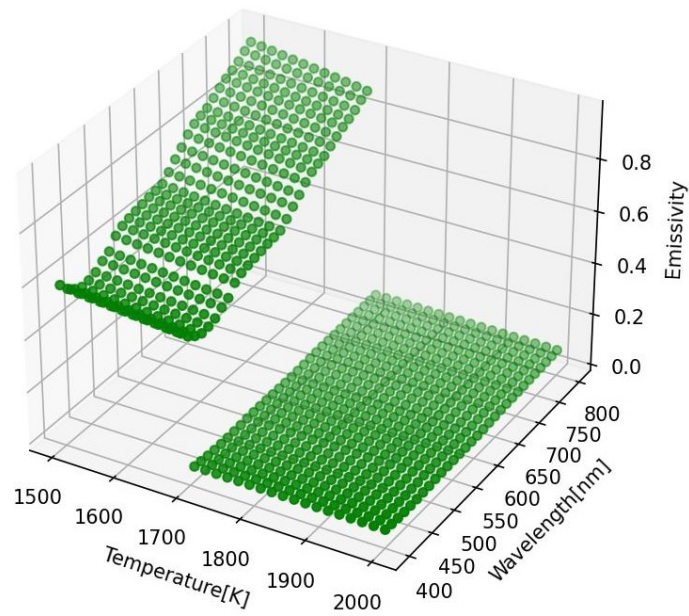


Figure 14: Emissivity value along wavelength and temperature calculated from model 9

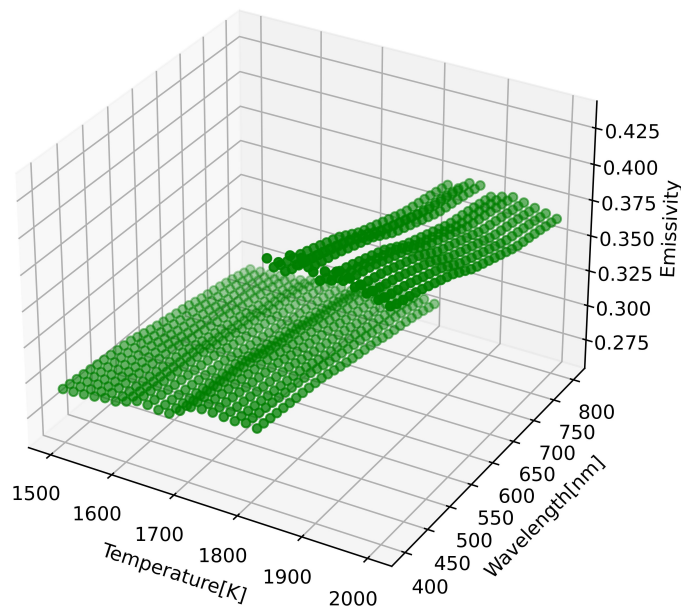


Figure 15: Emissivity value along wavelength and temperature of iron[15], [16]

small variation with changing wavelengths. Consequently, introducing emissivity data from real materials for verification is deemed necessary.

4.1.3 Camera model

After obtaining the temperature field and emissivity model of hypothetical material, the physical value of spectral radiation intensity should be calculated, then, the physical value of spectral radiation intensity is converted to digital value using camera model, which is the output of the complete virtual experiment platform.

To ensure consistency and scalability within the program for future feature additions, all calculations in the program are conducted using metric units. For instance, temperature is measured in Kelvin, and wavelength is measured in meters. Therefore, it is crucial to note that the unit of wavelength in the camera model's calculations is meters, not nanometers. This ensures dimensional correctness throughout the integration process.

As mentioned in Fig.7, the camera model is based on an integration method, which integrate the spectral intensity received by the sensor along the specific range of wavelength. However, due to the varying quantum efficiency of each channel in sensor, it means that for a virtual camera with 8 channels, each pixel requires 8 independent integration operations. This operation requires a large computational effort. So, in order to accelerate the generation speed and thus reduce the time cost of virtual experiment platform, a parallel computing strategy is introduced.

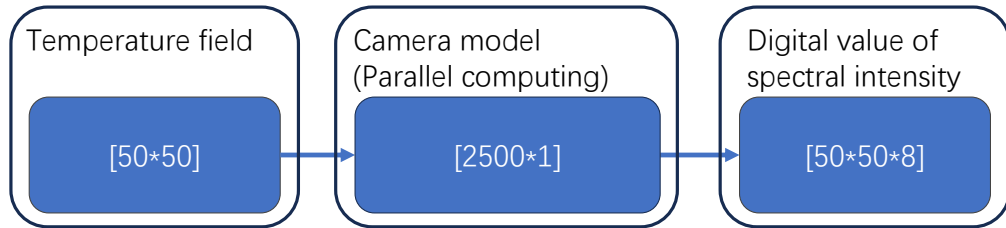


Figure 16: Shape of array used in camera model

The essence of parallel computing lies in decomposing a complex task into multiple tasks and utilizing multithreading techniques to execute these computational tasks simultaneously on different cores of the CPU. In this context, the camera model treats the integral computation on each pixel as an individual task, thereby significantly improving CPU utilization and substantially reducing computational time[17]. To facilitate task partitioning, the dimension of the temperature field mentioned earlier in this section needs to be reduced, from a 50×50 matrix to a one-dimensional array of size 2500×1 . This allows for obtaining 2500 parallel tasks. Once the calculations are completed, the resulting matrix of size 2500×8 is then transformed back into a three-dimensional matrix of size $50 \times 50 \times 8$. In this manner, a digital value similar to the data obtained in real experiments is computed.

4.2 Temperature estimation algorithm

After obtaining the digital value of spectral radiation intensity, the tasks of this virtual experiment platform are considered complete, and the next step involves data processing

and calculations. The core of the temperature estimation algorithm lies in reconstructing the physical value of spectral radiation intensity based on the known digital values and the chosen parameters. Subsequently, through the implementation of a curve fitting algorithm, the estimated emissivity and temperature can be calculated.

4.2.1 Rebuild physical value of spectral radiation intensity

Hence, it is evident that the process of reconstructing the physical value holds significant importance in the temperature estimation algorithm. This reconstruction process represents the conversion of spectral radiation intensity from its physical value to a digital value. By analyzing the reconstructed results, the relationship between the physical value (I_{rec}) and the parameters (T, k) to be fitted can be established, where T and k are derived from Eq.3.7. Subsequently, by performing curve fit algorithm between the reconstructed physical value and the experimental data, we can obtain the parameters (T, k) that best fit the real data. Therefore, it becomes apparent that the reconstruction of the physical value can affect the accuracy of the temperature prediction algorithm discussed in this thesis.

As mentioned in Eq.3.7, the reconstructed physical value of spectral radiation intensity is generated based on the integration method. It can be observed that the digital value can be considered as a function of temperature of hypothetical material T and parameters of emissivity model k .

$$I_{rec}^i(k, T) = q \int B(\lambda, T) \cdot \varepsilon(\lambda, k, T) \cdot \eta_{camera}^i d\lambda \quad (4.8)$$

Eq.4.8 shows the mathematical expression of reconstructed physical value of spectral radiation intensity of i_{th} channel. So, the current objective is to minimize the cost in Eq.3.8 by optimizing the values of k and T . In other words, the goal is to make the reconstructed spectral radiation intensity $I_{rec}(k, T)$ as close as possible to the values obtained in virtual experiments. By minimizing the cost function, the temperature estimation algorithm aims to achieve a high level of accuracy and fidelity in calculating the temperature based on the reconstructed digital values.

4.2.2 Emissivity model used for calculation

In the previous section, it is evident that the temperature estimation algorithm is essentially performing a curve fit algorithm on the parameters of the emissivity model and temperature of the hypothetical material. Therefore, the choice of the emissivity model significantly impacts the accuracy of the temperature estimation algorithm. In order to enhance the generality of this temperature prediction algorithm and prevent overfitting, a hypothesis is proposed: the temperature prediction algorithm is unaware of the material's emissivity characteristics. Hence, it is necessary to use a different emissivity model from the one used in the virtual experiment platform to reconstruct the digital value of spectral radiation intensity.

Based on mentioned above, the temperature estimation algorithm introduced in this paper tested several different emissivity models, namely:

1. Linear model
2. Linear square model
3. Quadratic model

4. Exponential model
5. A combined model composed of the linear square and exponential models

These models are distinguished based on the relationship between emissivity and wavelength. Each model represents a different mathematical expression that describes how emissivity varies with wavelength. In order to simplify the calculation process and thus set boundary conditions of parameters k in emissivity model, all wavelength used in this emissivity model is normalized wavelength λ_{norm} . The mathematical expression can be described as followed:

$$\lambda_{norm} = \frac{\lambda - \lambda_{lb}}{\lambda_{ub} - \lambda_{lb}} \quad (4.9)$$

To enhance the readability of the formula, the parameter k in Eq.4.8 is written in vector form in Eq.4.10 based on the number of parameters in emissivity model.

$$k = \begin{pmatrix} a \\ b \\ c \end{pmatrix} \text{ or } \begin{pmatrix} a \\ b \end{pmatrix} \quad (4.10)$$

With the lower boundary of wavelength $\lambda_{lb} = 500nm$ and the upper boundary of wavelength $\lambda_{ub} = 1000nm$. Thus, the input of the emissivity model used in temperature estimation algorithm is thus dimensionless number.

Linear model

Linear model refers to a linear relationship between emissivity and wavelength, which could be written as Eq.4.11:

$$\varepsilon(\lambda) = a \cdot \lambda_{norm} + b \quad (4.11)$$

The linear model represents the simplest and most straightforward emissivity model. It provides an easy way to visualize the calculated emissivity model and reduces complexity in defining various boundary conditions within the emissivity model.

Linear square model

The linear square model is distinct from the linear model, as it incorporates three parameters representing the coefficients of the quadratic term, the linear term, and the constant term. Its mathematical expression can be described as Eq.4.12:

$$\varepsilon(\lambda) = a \cdot \lambda_{norm}^2 + b \cdot \lambda_{norm} + c \quad (4.12)$$

The linear square model can be used to describe more intricate emissivity models for materials. With an additional parameter compared to the previous linear model, it offers increased degrees of freedom for curve fitting, enabling a better fit to complex shapes. Nevertheless, the augmented complexity may also lead to a higher risk of overfitting as well as increase of computational demand required.

Quadratic model

Consequently, in order to simplify the computation of the linear square model, the quadratic model was introduced. In this model, the coefficient of the linear term in the original linear square model is set to 0. This simplification leads to a reduction in the number of parameters within the emissivity model. The emissivity model can be expressed as Eq.4.13

$$\varepsilon(\lambda) = a \cdot \lambda_{norm}^2 + b \quad (4.13)$$

Exponential model

In the exponential model, emissivity is exponentially related to wavelength. Due to the monotonic nature of the exponential function, this model enhances the accuracy of parameter estimation along the gradient descent of the cost function during curve fitting, thereby improving the computational efficiency. The mathematical expression can be expressed in Eq.4.14:

$$\varepsilon(\lambda) = \exp(-a \cdot \lambda_{norm} - b) \quad (4.14)$$

For materials commonly used in PBF-LB/M, emissivity tends to decrease with increasing wavelength. Therefore, to reduce the range of parameters during curve fitting, the exponent term $a \cdot \lambda_{norm} + b$ was set as non-negative value.

Mixed model

This model is a combination of two models. In Fig.14, it can be observed that the emissivity of the virtual material undergoes significant changes when the temperature exceeds the material's melting point, and the emissivity variations become smaller in the liquid phase. Therefore, when emissivity changes are relatively small, i.e., when the material is in the liquid phase, the exponential model is more suitable. On the other hand, when emissivity changes are more pronounced, i.e., when the material is in the solid phase, the linear square model is more appropriate. This approach not only improves the computational accuracy of the model in the solid region but also ensures the computational efficiency of the model in the liquid region.

In this model, the computation starts with the linear square model. The computed results are then filtered to identify points where the temperature exceeds the material's melting point. Subsequently, the exponential model is utilized to recompute the emissivity and temperature for those specific points. Finally, the results from both calculations are combined to obtain a higher precision outcome. However, this process demands higher computational resources. Consequently, it is observed that this model significantly increases the computational time required for temperature estimation algorithms.

4.2.3 Curve fit algorithm

After obtaining the reconstructed physical values of intensity, a curve fit algorithm is required to determine temperature and the parameters of the emissivity model that best align with the actual received intensity. However, in this work, both the data obtained from the virtual experimental platform and the data from real experiments are not continuous spectral intensities. Conversely, the input for this temperature estimation algorithm is a two-dimensional array with dimensions of 8x2, which can be regarded as 8 samples of a continuous physical value.

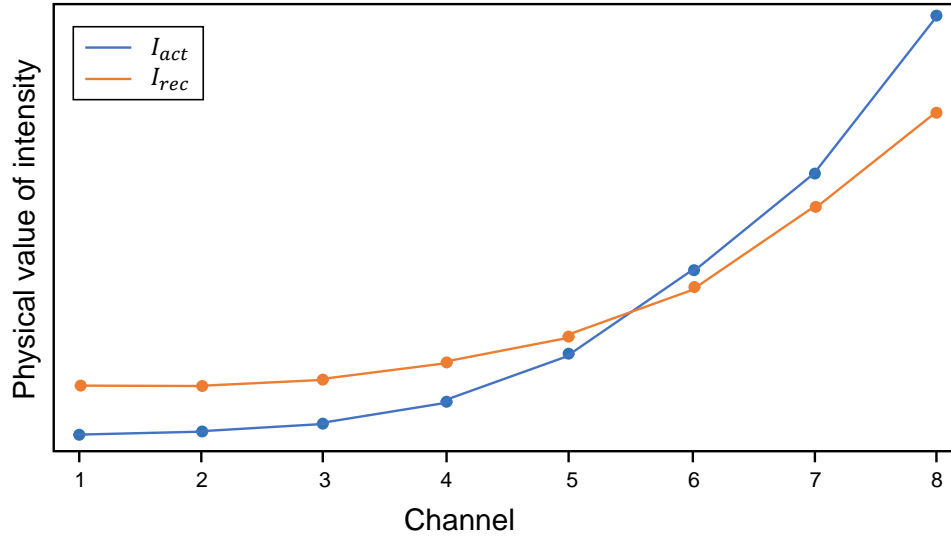


Figure 17: Comparison between actual received intensity I_{act} and reconstructed intensity I_{rec} of one point

Fig.17 illustrates the reconstructed physical value for each channel and the corresponding physical values from the original experimental data. It is evident that this approach simplifies the visualization of independent channel data and facilitates the utilization of this profile for curve fitting purposes.

4.2.4 Parameters in temperature estimation algorithm

The temperature estimation algorithm uses numerous parameters, which significantly impact the precision and consistency of the computed results. Therefore, it is essential to set boundary conditions for these parameters.

Wavelength range

In Fig.6, it can be observed that the total quantum efficiency of the sensor η_{camera} decreases to 0 when the radiation wavelength exceeds 900 nanometers. This effect is attributed to the presence of a filter on the sensor. Consequently, when reconstructing the physical values of the spectral radiation intensity, the integration limits are set to be within the range of 500 nanometers to 1000 nanometers. This approach ensures that the essential information is captured while reducing the computational resources required for integration and thus improving the computational speed.

Boundary condition of estimated temperature

In the temperature estimation algorithm, the process starts with an initial guess, which is used to perform the first reconstruction of the physical values of the spectral radiation intensity. This reconstruction yields a cost function and a gradient that minimizes the cost function. The algorithm then adjusts the parameters to be optimized along this gradient before proceeding to the next iteration. It is evident that the choice of the initial guess significantly influences the computational efficiency of the program and can help avoid potential physically meaningless local minima.

To address this, it is mandated that the predicted temperature in the temperature estimation

algorithm lie within the range of 500 to 2000K. This constraint ensures that the algorithm operates within a physically meaningful and relevant temperature range, preventing unrealistic results and potentially leading to a more effective and efficient optimization process.

Boundary condition of estimated emissivity

Unlike the boundary conditions applied to the estimated temperature, the boundaries for emissivity are much narrower. This is due to the physical definition of emissivity mentioned earlier in the text. Therefore, it is necessary to apply a boundary condition of $0 < \varepsilon < 1$ for emissivity during the calculations. However, in the curve fit algorithm mentioned in this work, emissivity is not a variable to be determined. Hence, it becomes necessary to incorporate this boundary condition directly into the emissivity model.

5 Calculation results and analysis

Once all the experiment data and parameters are determined, the results of the calculation should be presented and analyzed. Thus, the accuracy, consistency, pros and cons of the virtual experiment platform and temperature estimation algorithm can be systematically analyzed.

5.1 Calculation results

In virtual experiment platform and temperature estimation algorithms, emissivity is considered as a function of radiation wavelength and temperature. Consequently, it varies with changes in temperature and radiation wavelength. This variability is advantageous for enhancing algorithm precision but introduces difficulties in visualizing computation results. Furthermore, temperature estimation algorithm doesn't directly calculate the emissivity of materials; instead, the algorithm optimize the parameters k of the emissivity model. Thus, the emissivity data of each point is a function of wavelength λ and thus cannot be directly visualized. To address this, a simplified approach for visualizing emissivity is introduced, which allows for a more intuitive representation of emissivity without compromising the accuracy of the computational process.

$$\varepsilon_{sim} = \overline{\varepsilon(\lambda)} \quad (5.1)$$

Eq.5.1 presents the mathematical expression for this simplification. ε_{sim} represents the simplified emissivity value, and $\varepsilon(\lambda)$ denotes the emissivity model's value at wavelength λ . In other words, in this work, the visualization of emissivity is derived from the average value of emissivity model data within the wavelength range of 500 to 1000 nanometers.

By employing the same simplification method in the generation of experimental data and subsequent temperature estimation algorithm, the validity of the program's verification is ensured. This consistency guarantees that the comparison between the data used for validation remains effective and reliable throughout the process.

After obtaining a standardized emissivity visualization method, it is necessary to validate the calculation results. For the convenience of validation, several data that cannot be obtained in real experiments, such as temperature and emissivity of hypothetical material have been saved in several files in the virtual experiment platform and used to check the accuracy in validation process.

5.1.1 Raw experiment data from virtual experiment platform

In order to assess the performance of the temperature estimation algorithm at different temperatures and facilitate visual analysis, a linear temperature distribution is employed during the validation process. The background temperature is set to 1000K, while the center point's temperature is set at 1900K. Details is shown in Fig.18. Simultaneously, the melting point of the hypothetical material is defined as 1600K (except black body and gray body hypothetical material). This approach allows for the comparison of data obtained from the virtual experimental platform with that from real experiments, while checking

the accuracy of the temperature estimation algorithm in both solid and liquid phase of the hypothetical material.

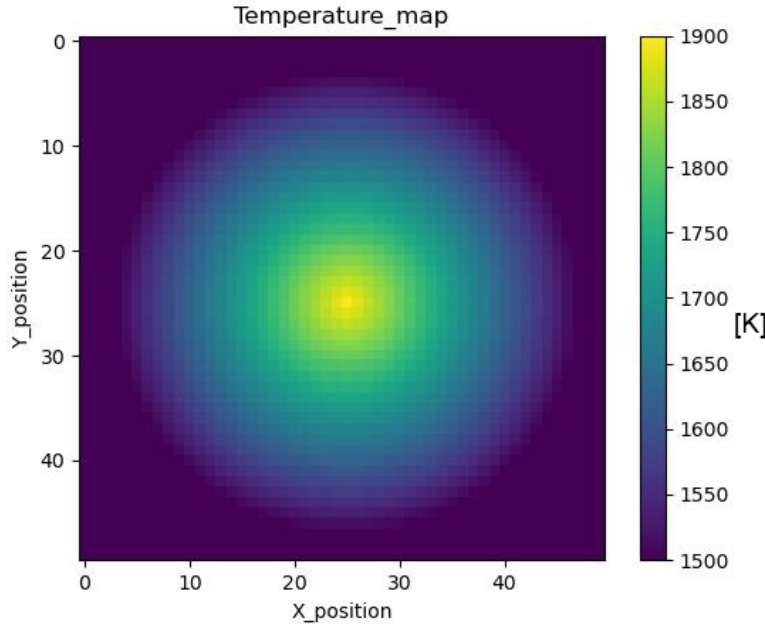


Figure 18: Temperature field used in validation

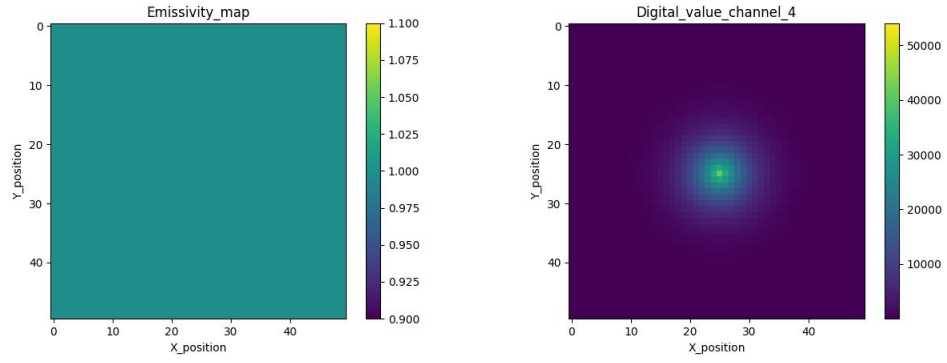
After obtaining a temperature field, the virtual experimental platform used the aforementioned 12 different emissivity models to generate 12 different sets of experimental data. This approach simulated the radiative behavior of 12 hypothetical materials under identical temperature conditions in the virtual experiment platform.

As a result, Fig.19 displays the emissivity fields generated by different model along with their corresponding radiation intensities. To conserve space, digital values of channel 4 in each experiment data were chosen as representatives of the intensity data.

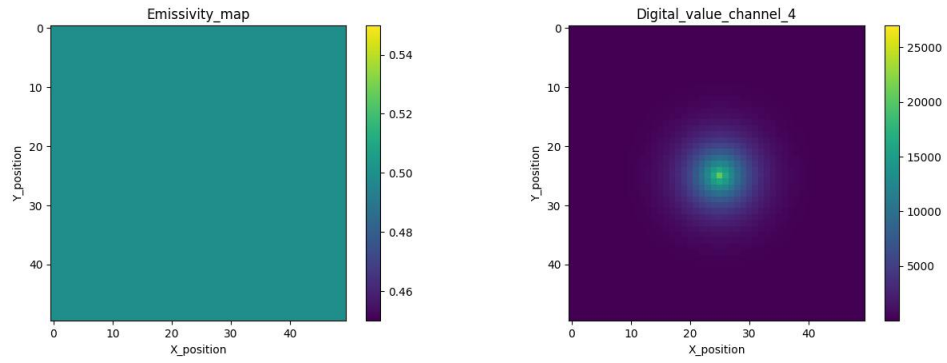
It can be observed that in blackbody and gray body materials, emissivity is not dependent on the material's temperature or status. As a result, the emissivity field exhibits a uniform color distribution. This characteristic also leads to a situation in the calculation of radiation intensity, where the physical values received by the virtual camera show a maximum at the center point and decrease as the temperature decreases.

However, in more general material models, such as Model 1 and Model 8, emissivity undergoes a discontinuity when the material transitions from the solid state to the liquid state. This is due to the fact that the emissivity of liquid phase is smaller than that of solid phase. Consequently, the radiation intensity received by the virtual camera decreases at the boundary when the material changes from solid to a liquid. Subsequently, at the center point, the radiation intensity emitted by the hypothetical material increases again due to the rise in temperature. This phenomenon results in a bright halo appearing in the digital value of channel 4 in the images. The center of this halo exhibits a point with higher brightness level.

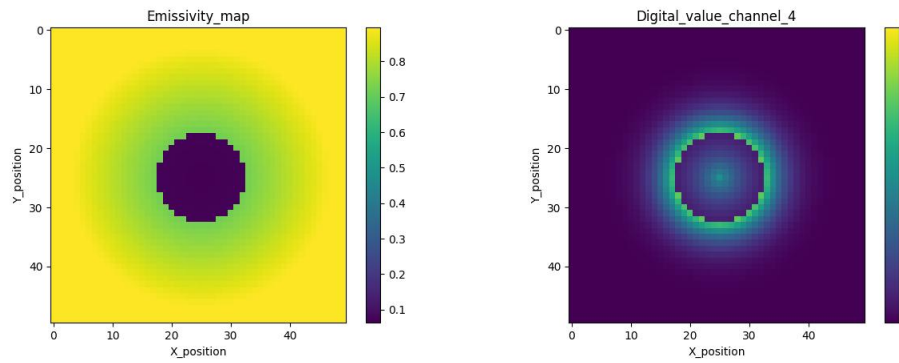
Indeed, the non-uniform intensity distribution caused by different emissivity characteristics of materials can lead to challenges for the subsequent temperature estimation algorithm. The intensity distribution along wavelength differs due to the different emissivity model of the hypothetical material. Consequently, in the curve fit algorithm, the most suitable



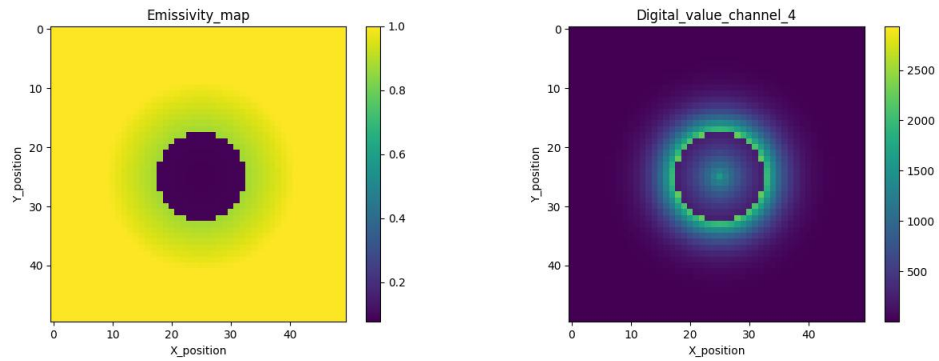
(a) Black body



(b) Gray body



(c) Model 1



(d) Model 8

Figure 19: Emissivity field and digital value of radiation intensity in channel 4 for black body material(a), gray body material(b), material based on model 1(c) and model 8(d)

emissivity model for the current material may change accordingly. Therefore, particular attention should be given to the phase transition of the hypothetical material in the context of temperature estimation.

After investigating the impact of different emissivity models on material radiative characteristics, it is necessary to explore the relationship between digital values of radiation intensity across different channels. Fig.20 displays the images of a material based on Model 1 at a temperature of 1900K, captured using 8 different channels. In this image, it can be observed that the intensity received by the virtual camera increases with the channel number.

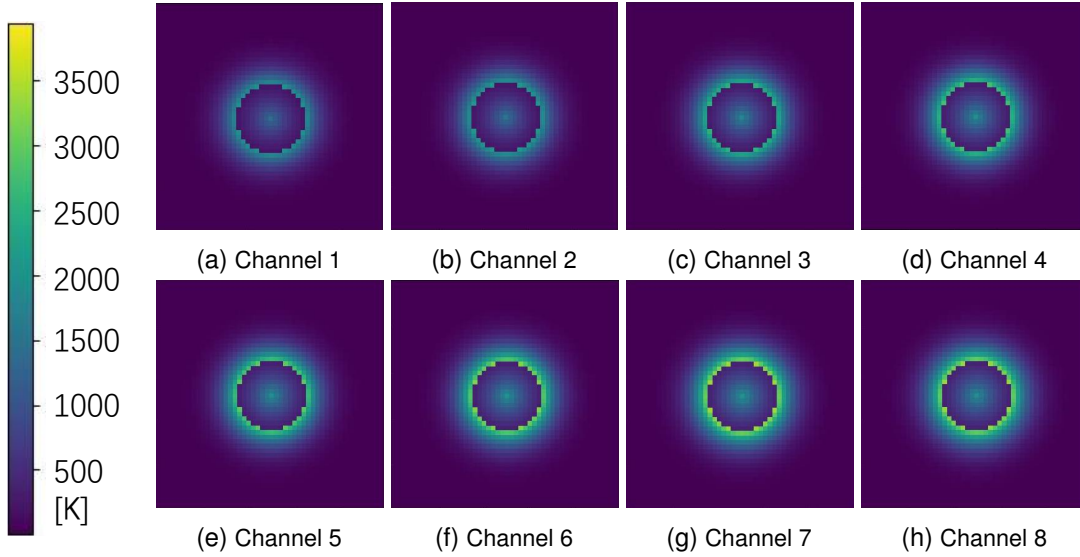


Figure 20: Digital value of each channel by hypothetical material based on model 1 and a linear temperature distribution with center temperature 1900K

According to Wien's displacement law introduced in previous chapter, as described in Eq.3.3, when the hypothetical material's temperature is 1900K, it is easy to calculate the peak wavelength (λ_{peak}) as 1525nm. Consequently, it can be inferred that the spectral intensity of blackbody radiation emitted by the hypothetical material will increase with increasing wavelength across the entire observation range (500 – 1000nm). This characteristic aligns with the real experimental observation, where the spectral radiation intensity received by a camera increases with the channel number.

5.1.2 Estimated temperature field and emissivity field

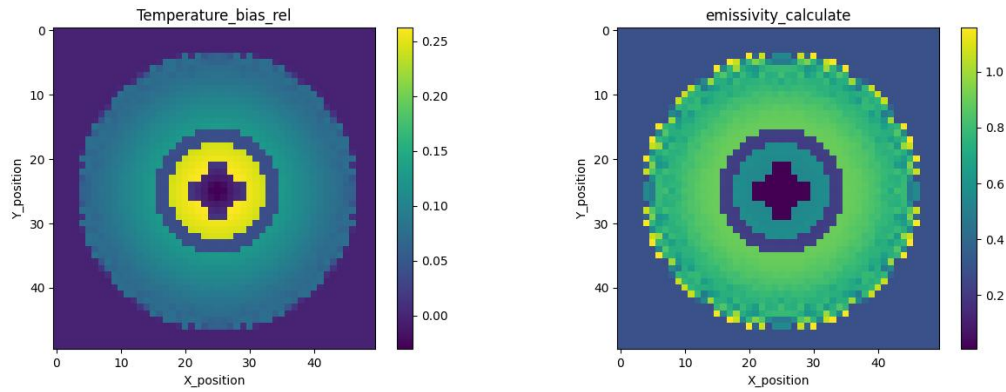
After obtaining reliable experimental data, it is essential to perform temperature estimation algorithm to validate the accuracy of the temperature estimation algorithm. The temperature estimation algorithm will yield two primary results: the estimated temperature field and the simplified estimated emissivity field. These computational results will be presented:

1. Estimated temperature field: The estimated temperature field represents the spatial distribution of temperature across the observation area. This is a most important output of the whole temperature estimation algorithm.
2. Simplified estimated emissivity field: The simplified estimated emissivity field denotes the variation of emissivity across the observation area. It could be used to identify

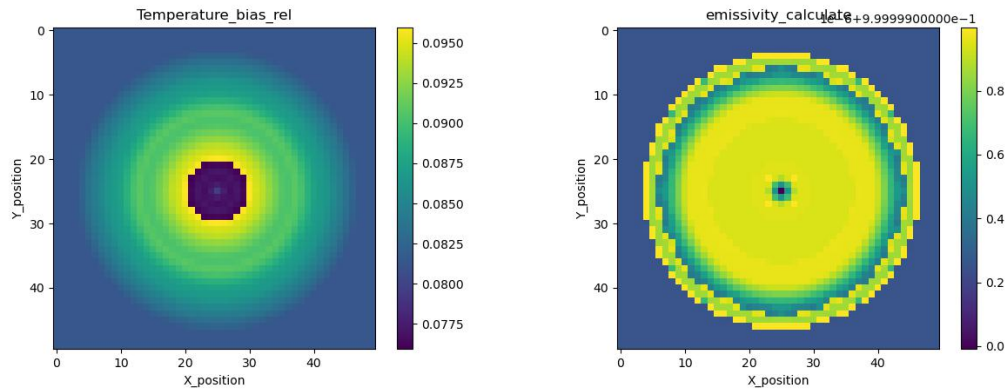
the phase change area and thus find the improvement potential.

For visualization, the presentation of the computational results will be categorized based on the emissivity model used in the temperature estimation algorithm. As the experimental data for these temperature estimation algorithm use the same temperature distribution, relative error of temperature is employed here to represent the accuracy of the computations. To save space, the results of calculations for blackbody materials and materials based on Model 7 are selected for presentation.

Linear model



(a) Material based on model 1



(b) Material based on real iron data

Figure 21: Calculation results of linear model

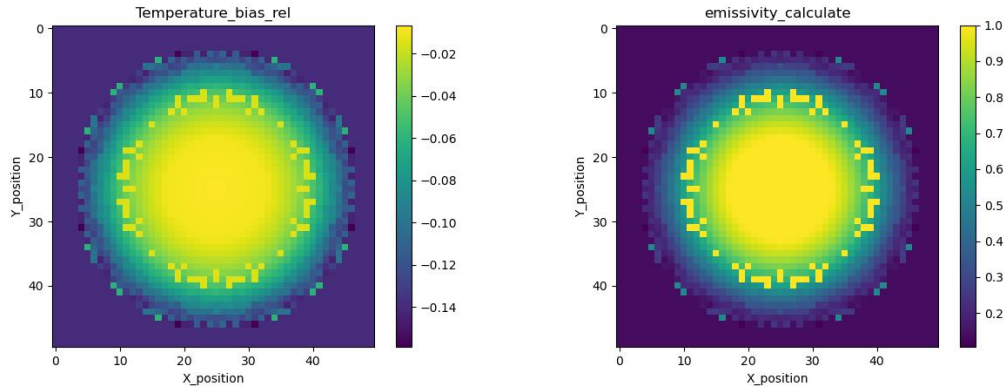
Fig.21 demonstrate the calculation result on material based on model 7 and real data from iron. It can be found that the calculation result is more stable in real data due to the material character.

More calculation result can be found in table ??.

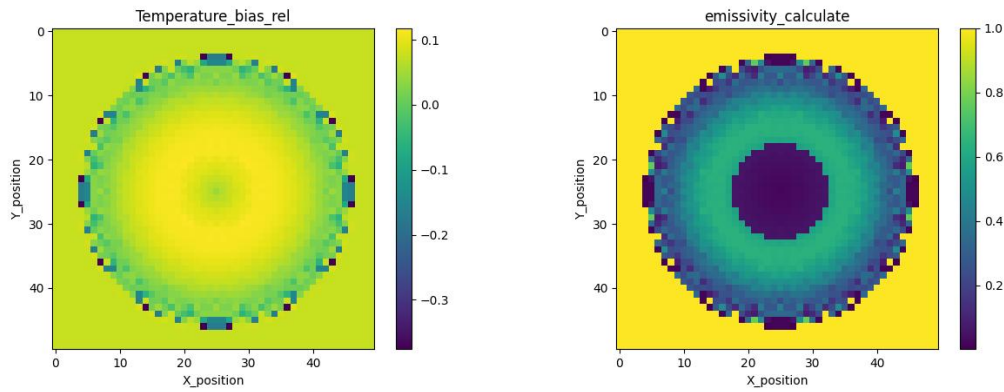
It can be observed that in the computation of linear models, calculation results based on real data exists relatively low average relative error and the lowest standard deviation. This indicates that the linear model maintains a higher level of consistency when performing calculations on real materials. It also achieves a maximum relative error of no more than 9.6%. However, when performing calculations on other hypothetical materials, the linear model may produce relatively large errors, particularly for model 8, which has a high

standard deviation, meaning the low consistency in the calculations. As mentioned in previous sections, this decrease in computational consistency could be attributed to the fact that the emissivity of materials based on model 8 undergoes a sudden change as the wavelength increases, which is a potential reason for the decline in calculation consistency.

Linear square model



(a) Black body material



(b) Material based on model 7

Figure 22: Calculation results of linear square model

Quadratic model

not finished

Exponential model

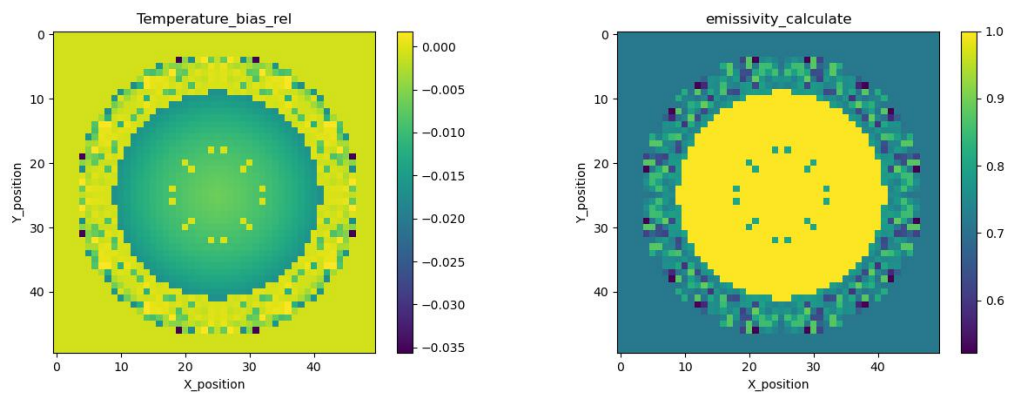
not finished

Mixed model

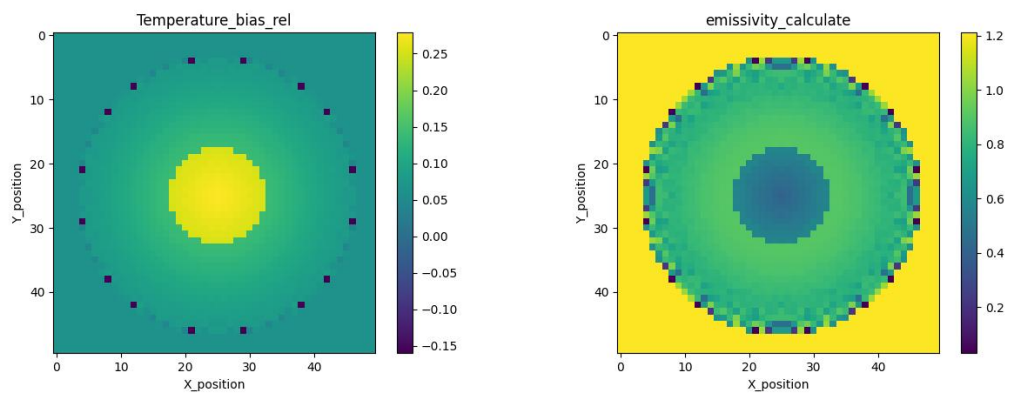
In this mixed model, the computational time has significantly increased due to the utilization of two different emissivity models.

5.1.3 Statistical results

After obtaining all calculation results, some statistical results can be found in tabel 1.

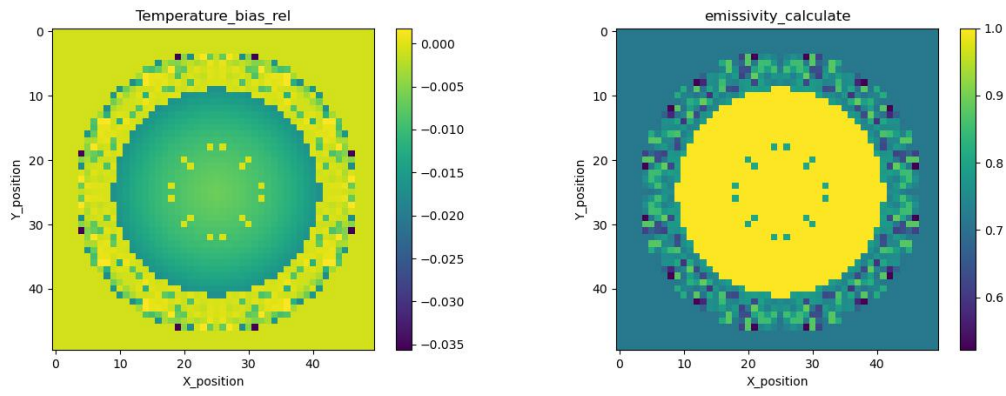


(a) Black body material

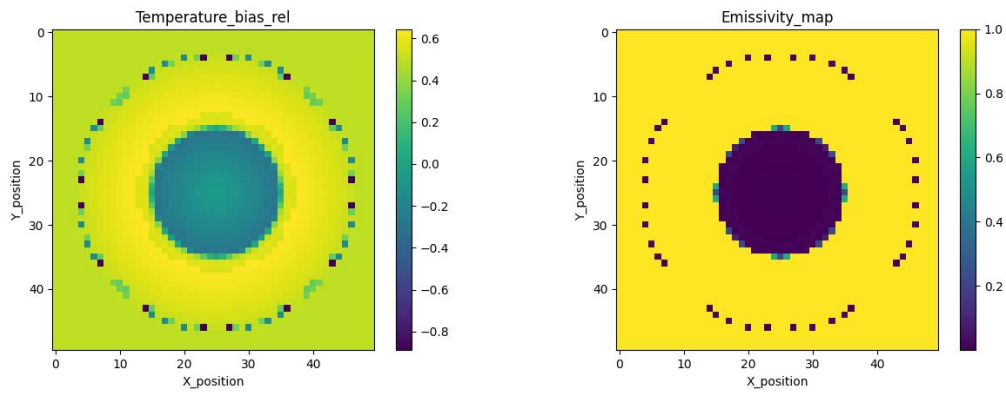


(b) Material based on model 7

Figure 23: Calculation results of quadratic model

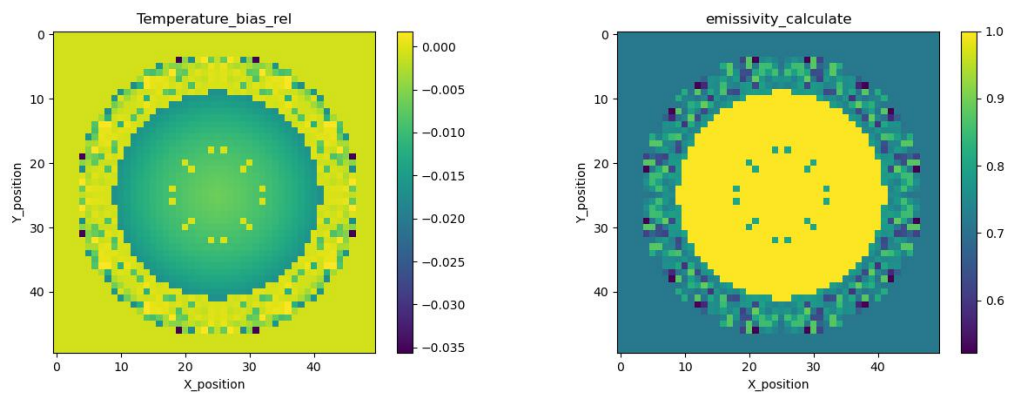


(a) Black body material

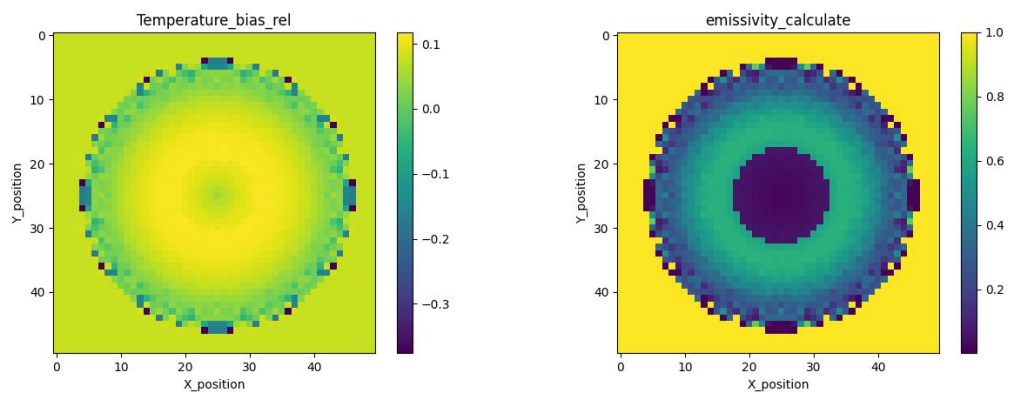


(b) Material based on model 7

Figure 24: Calculation results of exponential model



(a) Black body material



(b) Material based on model 7

Figure 25: Calculation results of mixed model

Table 1: Calculation results from different models

	Black body	Real data	Model 1	Model 2	Model 3	Model 4	Model 5	Model 6	Model 7	Model 8	Model 9
Linear											
Abs. difference [K]	-30.3	-142.3	-247.6	-303.1	-285.7	-255.8	-325.4	-344.8	-460.1	-16.087	-301.8
Rel. difference	0.13	0.08	0.18	0.19	0.18	0.18	0.20	0.21	0.28	0.16	0.19
SD [K]	289.13	13.20	212.46	143.79	150.88	199.79	104.78	75.32	104.75	290.48	112.95
Max. difference [K]	0.717	0.096	0.322	0.323	0.312	0.322	0.312	0.316	0.378	0.342	0.311
Min. difference [K]	0.001	0.076	0.001	0.0001	0.001	0.002	0.019	0.104	0.004	0.003	0.009
Quadratic											
Abs. difference [K]	-30.3	-142.3	-247.6	-303.1	-285.7	-255.8	-325.4	-344.8	-460.1	-16.087	-301.8
Rel. difference	0.13	0.08	0.18	0.19	0.18	0.18	0.20	0.21	0.28	0.16	0.19
SD [K]	289.13	13.20	212.46	143.79	150.88	199.79	104.78	75.32	104.75	290.48	112.95
Max. difference [K]	0.717	0.096	0.322	0.323	0.312	0.322	0.312	0.316	0.378	0.342	0.311
Min. difference [K]	0.001	0.076	0.001	0.0001	0.001	0.002	0.019	0.104	0.004	0.003	0.009
Linear square											
Abs. difference [K]	-30.3	-142.3	-247.6	-303.1	-285.7	-255.8	-325.4	-344.8	-460.1	-16.087	-301.8
Rel. difference	0.13	0.08	0.18	0.19	0.18	0.18	0.20	0.21	0.28	0.16	0.19
SD [K]	289.13	13.20	212.46	143.79	150.88	199.79	104.78	75.32	104.75	290.48	112.95
Max. difference [K]	0.717	0.096	0.322	0.323	0.312	0.322	0.312	0.316	0.378	0.342	0.311
Min. difference [K]	0.001	0.076	0.001	0.0001	0.001	0.002	0.019	0.104	0.004	0.003	0.009
Exponential											
Abs. difference [K]	-30.3	-142.3	-247.6	-303.1	-285.7	-255.8	-325.4	-344.8	-460.1	-16.087	-301.8
Rel. difference	0.13	0.08	0.18	0.19	0.18	0.18	0.20	0.21	0.28	0.16	0.19
SD [K]	289.13	13.20	212.46	143.79	150.88	199.79	104.78	75.32	104.75	290.48	112.95
Max. difference [K]	0.717	0.096	0.322	0.323	0.312	0.322	0.312	0.316	0.378	0.342	0.311
Min. difference [K]	0.001	0.076	0.001	0.0001	0.001	0.002	0.019	0.104	0.004	0.003	0.009
Mixed model											
Abs. difference [K]	-30.3	-142.3	-247.6	-303.1	-285.7	-255.8	-325.4	-344.8	-460.1	-16.087	-301.8
Rel. difference	0.13	0.08	0.18	0.19	0.18	0.18	0.20	0.21	0.28	0.16	0.19
SD [K]	289.13	13.20	212.46	143.79	150.88	199.79	104.78	75.32	104.75	290.48	112.95
Max. difference [K]	0.717	0.096	0.322	0.323	0.312	0.322	0.312	0.316	0.378	0.342	0.311
Min. difference [K]	0.001	0.076	0.001	0.0001	0.001	0.002	0.019	0.104	0.004	0.003	0.009
Mixed model											
Abs. difference [K]	-30.3	-142.3	-247.6	-303.1	-285.7	-255.8	-325.4	-344.8	-460.1	-16.087	-301.8
Rel. difference	0.13	0.08	0.18	0.19	0.18	0.18	0.20	0.21	0.28	0.16	0.19
SD [K]	289.13	13.20	212.46	143.79	150.88	199.79	104.78	75.32	104.75	290.48	112.95
Max. difference [K]	0.717	0.096	0.322	0.323	0.312	0.322	0.312	0.316	0.378	0.342	0.311
Min. difference [K]	0.001	0.076	0.001	0.0001	0.001	0.002	0.019	0.104	0.004	0.003	0.009

5.2 Data analysis

use statistical method to analyse the calculated result

5.2.1 Sensitivity analysis of emissivity models

how different emissivity model affect the performance

5.2.2 Performance between different materials

how is the performance between different materials.

6 Conclusion and prospects

A Appendices

Hello, here is some text without a meaning. This text should show what a printed text will look like at this place. If you read this text, you will get no information. Really? Is there no information? Is there a difference between this text and some nonsense like “Huardest gefburn”? Kjift – not at all! A blind text like this gives you information about the selected font, how the letters are written and an impression of the look. This text should contain all letters of the alphabet and it should be written in of the original language. There is no need for special content, but the length of words should match the language.

This is the second paragraph. Hello, here is some text without a meaning. This text should show what a printed text will look like at this place. If you read this text, you will get no information. Really? Is there no information? Is there a difference between this text and some nonsense like “Huardest gefburn”? Kjift – not at all! A blind text like this gives you information about the selected font, how the letters are written and an impression of the look. This text should contain all letters of the alphabet and it should be written in of the original language. There is no need for special content, but the length of words should match the language.

And after the second paragraph follows the third paragraph. Hello, here is some text without a meaning. This text should show what a printed text will look like at this place. If you read this text, you will get no information. Really? Is there no information? Is there a difference between this text and some nonsense like “Huardest gefburn”? Kjift – not at all! A blind text like this gives you information about the selected font, how the letters are written and an impression of the look. This text should contain all letters of the alphabet and it should be written in of the original language. There is no need for special content, but the length of words should match the language.

After this fourth paragraph, we start a new paragraph sequence. Hello, here is some text without a meaning. This text should show what a printed text will look like at this place. If you read this text, you will get no information. Really? Is there no information? Is there a difference between this text and some nonsense like “Huardest gefburn”? Kjift – not at all! A blind text like this gives you information about the selected font, how the letters are written and an impression of the look. This text should contain all letters of the alphabet and it should be written in of the original language. There is no need for special content, but the length of words should match the language.

Hello, here is some text without a meaning. This text should show what a printed text will look like at this place. If you read this text, you will get no information. Really? Is there no information? Is there a difference between this text and some nonsense like “Huardest gefburn”? Kjift – not at all! A blind text like this gives you information about the selected font, how the letters are written and an impression of the look. This text should contain all letters of the alphabet and it should be written in of the original language. There is no need for special content, but the length of words should match the language.

Bibliography

- [1] Frazier, W. E., “Metal additive manufacturing: A review”, *Journal of Materials Engineering and Performance*, vol. 23, no. 6, pp. 1917–1928, 2014, ISSN: 1544-1024. DOI: 10.1007/s11665-014-0958-z. [Online]. Available: <https://link.springer.com/article/10.1007/s11665-014-0958-z>.
- [2] Swift, K. G. and Booker, J. D., “Rapid prototyping processes”, in *Manufacturing process selection handbook*, Swift, K. G. and Booker, J. D., Eds., Amsterdam: Elsevier, 2013, pp. 227–241, ISBN: 9780080993607. DOI: 10.1016/B978-0-08-099360-7.00008-2.
- [3] Kruth, J. P., “Material increment manufacturing by rapid prototyping techniques”, *CIRP Annals*, vol. 40, no. 2, pp. 603–614, 1991, ISSN: 0007-8506. DOI: 10.1016/S0007-8506(07)61136-6. [Online]. Available: <https://www.sciencedirect.com/science/article/pii/S0007850607611366>.
- [4] Revilla-León, M., Meyer, M. J., and Özcan, M., “Metal additive manufacturing technologies: Literature review of current status and prosthodontic applications”, *International Journal of Computerized Dentistry*, pp. 55–67, 2019.
- [5] Oliveríra, J., LaLonde, A., and Ma, J., “Processing parameters in laser powder bed fusion metal additive manufacturing”, *Materials & Design*, vol. 193, p. 108762, 2020, ISSN: 0264-1275. DOI: 10.1016/j.matdes.2020.108762. [Online]. Available: <https://www.sciencedirect.com/science/article/pii/S0264127520302963>.
- [6] DebRoy, T., Wei, H. L., Zuback, J. S., Mukherjee, T., Elmer, J. W., Milewski, J. O., Beese, A. M., Wilson-Heid, A., De, A., and Zhang, W., “Additive manufacturing of metallic components – process, structure and properties”, *Progress in Materials Science*, vol. 92, no. 5, pp. 112–224, 2018, ISSN: 00796425. DOI: 10.1016/j.pmatsci.2017.10.001.
- [7] Li, D., Liu, R., and Zhao, X., *Overview of in-situ temperature measurement for metallic additive manufacturing: How and then what*, 2019. DOI: 10.26153/TSW/17384.
- [8] Hagqvist, P., Sikström, F., and Christiansson, A.-K., “Emissivity estimation for high temperature radiation pyrometry on ti-6al-4v”, *Measurement*, vol. 46, no. 2, pp. 871–880, 2013, ISSN: 02632241. DOI: 10.1016/j.measurement.2012.10.019.
- [9] Pixner, F., Buzolin, R., Schönfelder, S., Theuermann, D., Warchomicka, F., and Enzinger, N., “Contactless temperature measurement in wire-based electron beam additive manufacturing ti-6al-4v”, *Welding in the World*, vol. 65, no. 7, pp. 1307–1322, 2021, ISSN: 1878-6669. DOI: 10.1007/s40194-021-01097-0. [Online]. Available: <https://link.springer.com/article/10.1007/s40194-021-01097-0>.
- [10] Bammer, F., Holzinger, B., Humenberger, G., Schuöcker, D., and Schumi, T., “Integration of high power lasers in bending tools”, *Physics Procedia*, vol. 5, pp. 205–209, 2010, ISSN: 18753892. DOI: 10.1016/j.phpro.2010.08.045.
- [11] Kuhn, T. S., *Black-Body Theory and the Quantum Discontinuity, 1894-1912*. University of Chicago Press, 1987, ISBN: 9780226458007.
- [12] Fossum, E. R. and Hondongwa, D. B., “A review of the pinned photodiode for ccd and cmos image sensors”, *IEEE Journal of the Electron Devices Society*, vol. 2, no. 3, pp. 33–43, 2014. DOI: 10.1109/JEDS.2014.2306412.

- [13] Wang, N., Shen, H., and Zhu, R., “Constraint optimization algorithm for spectral emissivity calculation in multispectral thermometry”, *Measurement*, vol. 170, p. 108 725, 2021, ISSN: 02632241. DOI: 10.1016/j.measurement.2020.108725.
- [14] Taunay, P.-Y. C. R. and Choueiri, E. Y., “Multi-wavelength pyrometry based on robust statistics and cross-validation of emissivity model”, *The Review of scientific instruments*, vol. 91, no. 11, p. 114 902, 2020. DOI: 10.1063/5.0019847.
- [15] Kobatake, H., Khosroabadi, H., and Fukuyama, H., “Normal spectral emissivity measurement of liquid iron and nickel using electromagnetic levitation in direct current magnetic field”, *Metallurgical and Materials Transactions A*, vol. 43, no. 7, pp. 2466–2472, 2012, ISSN: 1073-5623. DOI: 10.1007/s11661-012-1101-0.
- [16] Watanabe, H., Susa, M., Fukuyama, H., and Nagata, K., “Phase (liquid/solid) dependence of the normal spectral emissivity for iron, cobalt, and nickel at melting points”, *International Journal of Thermophysics*, vol. 24, no. 2, pp. 473–488, 2003, ISSN: 1572-9567. DOI: 10.1023/A:1022924105951. [Online]. Available: <https://link.springer.com/article/10.1023/a:1022924105951>.
- [17] Asanovic, K., Bodik, R., Demmel, J., Keaveny, T., Keutzer, K., Kubitowicz, J., Morgan, N., Patterson, D., Sen, K., Wawrzynek, J., Wessel, D., and Yelick, K., “A view of the parallel computing landscape”, *Communications of the ACM*, vol. 52, no. 10, pp. 56–67, 2009, ISSN: 0001-0782. DOI: 10.1145/1562764.1562783.

List of Abbreviations

AM	Additive Manufacturing
CCD	Charge-coupled device
CMOS	Complementary Metal-oxide Semiconductor
LBAM	Professorship Laser-based Additive Manufacturing
MSI	Multispectral Imaging
PBF-LB/M	Laser-based Powder Bed Fusion of Metals
SLS	Selective Laser Sintering

Disclaimer

I hereby declare that this thesis is entirely the result of my own work except where otherwise indicated. I have only used the resources given in the list of references.

Garching, July 31, 2023

(Signature)